Journal of Power Sources 253 (2014) 397–403

Contents lists available at ScienceDirect

Journal of Power Sources

journal homepage: www.elsevier.com/locate/jpowsour

Development and characterization of a 280 cm^2 vanadium/oxygen fuel cell

Jens Noack*, Carsten Cremers, Domnik Bayer, Jens Tübke, Karsten Pinkwart

Applied Electrochemistry, Fraunhofer Institute for Chemical Technology, Joseph-von-Fraunhofer-Str. 7, 76327 Pfinztal, Germany

HIGHLIGHTS

- A vanadium/oxygen fuel cell with an active area of 280 cm^2 has been developed and tested.
- The cell uses 2 membranes to avoid side reactions on the platinum ORR catalyst.
- The cell performance has been compared to a 50 cm^2 design and had nearly similar values.
- In both cells, the performance was limited by slow oxygen reduction rate at room temperature.

ARTICLE INFO

Article history:
Received 19 July 2013
Received in revised form
21 November 2013
Accepted 14 December 2013
Available online 24 December 2013

Keywords:
Vanadium oxygen fuel cell
Vanadium air redox flow battery
Cell design
Voltammetry
Electrochemical impedance spectroscopy

ABSTRACT

A vanadium/oxygen fuel cell with an active area of 280 cm^2 has been developed. The cell consisted of two membranes with two half-cells and an intermediate chamber. The maximum achieved power density was 23 mW cm^{-2} at 0.56 V with lambda air = 3 and a 1.6 M V^{2+} solution at room temperature. The average discharge power density was 19.6 mW cm^{-2} at a constant current density of 40 mA cm^{-2} with an average voltage efficiency of 33%. The fuel based energy density was 18.2% of the theoretical value with 11.8 Wh L^{-1}. In comparison with a similarly constructed 50 cm^2 cell, both achieved similar performance levels. An analysis using the half-cell potential profiles and by means of impedance spectroscopy revealed that, as for the 50 cm^2 cell, the low rate of oxygen reduction reaction significantly affected the performance of the cell. Thus gives potential for the optimization of the cathode reaction and a reduction in the ohmic resistances potential for higher power densities.

1. Introduction

With a reduction in the production of crude oil with at the same time increasing demand, massive price increases are expected [1]. Motorized transport is almost exclusively tied directly or indirectly to the cheap availability of crude oil or natural gas. To have in the future low-cost alternatives available, currently intense research on alternative concepts is made. The most promising technology is the electro-mechanical propulsion of vehicles by the use of electro-chemical energy converters and -storage. Currently the biggest hurdle for broad market introduction is the availability of inexpensive electrochemical storage systems. In addition, there are other technology-related issues such as durability, reliability, recoverability, range (capacity), temperature behavior, etc. [2]. Batteries such as Lithium-Ion Batteries (LIB) do not have sufficiently high energy densities for longer distances with an acceptable amount of time, because a lot of the time must be used for recharging. Fast charge capable systems such as of spinel type $Li_4Ti_5O_{12}$ lithium titanate based LIBs have lower energy densities [3–5], require high, also fluctuating performance in an electrical grid with an increasing proportion of fluctuating energy sources. In contrast, fuel cells offer high energy densities [6] and acceptable lifetime. However, the use of hydrogen as an energy carrier requires complex, loss-prone and expensive handling, but the electro-chemical production process is well established by the electrolysis of water, methods such as the photocatalytic water splitting are in development [7]. An alternative could be systems in which electrical energy is stored by an energy converter in dissolved redox couples like redox flow batteries are [8,9]. The energy density of 20–80 Wh L^{-1}, based on the energy carrier fluid, is too low for mobile applications, but in general electrical regenerability and fast charge by changing the energy carrier fluids are given.

An often as vanadium redox flow battery or vanadium air oxygen fuel cell (VOFC) designated system uses dissolved vanadium ions as an energy source and oxygen as oxidant [10].

* Corresponding author. Tel.: +49 721 4640 870; fax: +49 721 4640 318.
E-mail address: jens.noack@ict.fraunhofer.de (J. Noack).

0378-7753/$ – see front matter © 2013 Elsevier B.V. All rights reserved.
http://dx.doi.org/10.1016/j.jpowsour.2013.12.070

The reaction equations are as follows:

$$\text{Anode}: V^{2+} \rightarrow V^{3+} + e^- \quad E^0 = -0.26\,\text{V} \tag{1}$$

$$\text{Cathode}: O_2 + 4H^+ + 4e^- \rightarrow 2H_2O \quad E^0 = +1.23\,\text{V} \tag{2}$$

$$\text{Cell reaction}: 4V^{2+} + O_2 + 4H^+ \rightarrow 4V^{3+} + 2H_2O \quad \Delta E = 1.49\,\text{V} \tag{3}$$

Here, the theoretical maximum energy density increased from 30 to 60 Wh L^{-1} compared to the vanadium redox flow battery (VRFB) by a factor of two, when using the same 1.6 M vanadium sulphate solution. Since the energy density in a VRFB is limited by the solubility of pentavalent VO_2^+ and the time-, concentration- and temperature-dependent formation of heteropolyacids by condensation, higher concentrations and thus energy densities in VOFCs could be realized with divalent and trivalent vanadium sulfate solutions. In addition to automotive applications also stationary applications are conceivable in which higher energy densities are desirable. In previous work different components and modes of operation with single cells and a 5-cell stack was studied [11]. A major challenge was the delamination of the catalyst layer of the catalyst coated membrane (CCM) by swelling, which could be reduced, however, so a 5-cell stack could be operated over a period of about 120 h. Hosseiny et al. reported a vanadium air redox flow battery (VARFB) called VOFC in which they exchanged the membrane electrode assembly (MEA) between charging and discharging with one having a different catalyst [12]. For discharge a platinum/carbon based (MEA) was used, for charging a titanium/iridium based was used. Our group reported an experimental comparison of a VOFC with a VRFB [13]. Like Menictas et al., we found a strong power loss during discharge of the cell and we attributed this to hydrogen evolution at the Pt-based catalyst by electro-migrated divalent vanadium, whereupon we developed a cell with two membranes to avoid this problem [14,15]. In this work we were interested in the upscaling of the cell and optimization of cell components to be able to build efficient cell stacks. Furthermore, we investigated operating parameters of the system, limitations and optimization possibilities. For more information about the causes of limitations, the values were compared with a 50 cm^2 cell, where in addition cathode-, anode- and redox potentials and -impedances were measured. We also wanted to provide more comparable data, for example energy- and power densities, impedances and potentials of cells and half-cells for further studies and developments.

2. Experimental

As shown in Fig. 1, a stackable design has been developed and a single cell was constructed with a geometric active area of 280 cm^2. The cell consisted of two half-cells separated by two membranes. Between the two membranes was a chamber in which a separate liquid could flow through. The anodic half-cell consisted of a PVC flow frame (d), a graphite foil (Sigracet TF6, SGL Carbon GmbH, Germany) and several layers of graphite felts (GFA5, SGL Carbon GmbH, Germany). The separation of the anodic half-cell was made by a NAFION® 115 membrane (DuPont, USA). The cathode half-cell consisted of a flow-through frame (h), a graphite foil, graphite felt (Sigracet TF6, GFA5, SGL Carbon GmbH, Germany), a gas diffusion layer (X0070, Freudenberg FCCT KG, Germany) and a catalyst coated membrane (CCM CC 0.6–0.8 mg cm^{-2} Pt on NAFION® 212, 20 wt% NAFION® ionomer in catalyst layer, Quintech GmbH, Germany). Between the two half-cells was a cavity formed by a flow frame (f), which was separated by the two membranes of anodic and cathodic half-cells. As a spacer, a graphite felt was placed in the cavity. The purpose of this cavity was to avoid the diffusion of divalent vanadium (V^{2+}) ions to the Pt-catalyst. V^{2+} solutions with their negative redox potential are not kinetically hindered on platinum electrodes and are rapidly oxidized by reduction of protons, which leads to the evolution of hydrogen and probably the delamination of the catalyst layer by the following reactions:

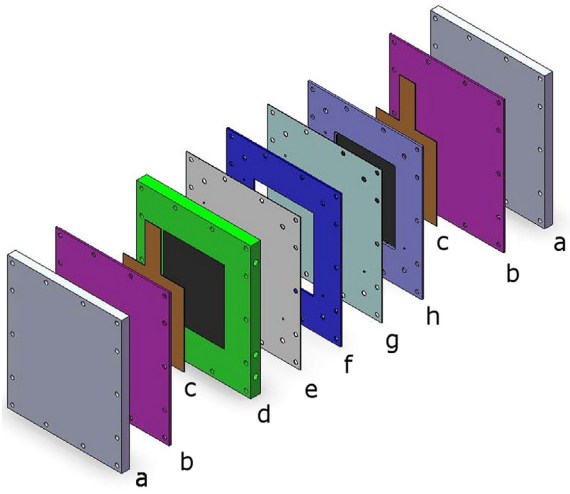

Fig. 1. 280 cm^2 VOFC components (a – end plate, b – isolation plate, c – current collector, d – anodic flow frame, e – membrane, f – gap flow frame, g – catalyst coated membrane, h – cathodic flow frame).

$$V^{2+} \rightarrow V^{3+} + e^- \quad E^0 = -0.26\,\text{V} \tag{4}$$

$$2H^+ + 2e^- \rightarrow H_2 \quad E^0 = 0.00\,\text{V} \tag{5}$$

$$2V^{2+} + 2H^+ \rightarrow 2V^{3+} + H_2 \quad \Delta E = 0.26\,\text{V} \tag{6}$$

Therefore the cavity was rinsed by a pump with 2 M sulfuric acid in cycle. The sulfuric acid was gassed externally with air to maintain the redox potential of the solution above a value of 0.1 V vs. NHE in order to oxidize any V^{2+} entering into V^{3+} to prevent the evolution of hydrogen gas at the cathode. Consequently over time a constant concentration of V^{3+} should reached in the cavity cycle with V^{3+} leaking to the cathode without causing hydrogen evolution.

Air at atmospheric pressure was used as the oxidant in the cathodic half-cell which was regulated by a mass flow controller. The anode cycle was filled with a defined amount of 1.6 M V^{2+} solution which was circulated by a pump through the graphite felts. The solution was prepared electrolytically in an electrolytic cell. A solution of 0.8 M $VOSO_4$, 0.4 M $V_2(SO_4)_3$, 2 M H_2SO_4 and 0.05 M H_3PO_4 (GFE-Metalle GmbH, Nürnberg, Germany) was electrolyzed until the catholyte redox potential was −1.1 V vs Hg/Hg_2SO_4. A cell with a geometric active area of 50 cm^2 was used, with a similar structure to the 280 cm^2 cell with a dynamic hydrogen electrode (DHE) on the cathode side of the CCM [16]. The DHE was employed during electrochemical impedance measurements. For these measurements a reference potential is required which is stable for the duration of the measurements of several minutes. To achieve the desired stability the DHE was covered with adhesive tape to prevent hydrogen removal and was operated at a current of 30 μA. Thus the potential of the DHE should be constant at about 0 V vs. RHE over the required period of time. Instead of graphite foils, graphite composite plates with thicknesses of 3 mm were used (FU 4396, Schunk Carbon GmbH, Germany). The CCM had a platinum loading of 1 mg cm^{-2} and 20 wt% NAFION® ionomer in the catalyst

layer (Baltic Fuel Cells GmbH, Germany). By the arrangement shown in Fig. 2, anode potential (φ_A), cathode potential (φ_C) and redox potential (φ_{NA}) of the V^{2+} solution where measured in addition to the cell voltage (φ_Z).

The electrochemical measurements were performed with a potentiostat (Gamry Reference 3000 + 8 channel electrometer, Gamry Instruments Inc., USA). The impedance measurements were carried out galvanostatically at an amplitude of 10 mA in a frequency range from 100 kHz to 0.01 or 0.1 Hz. In the 50 cm^2 cell, half-cell potentials, redox potentials and impedances were recorded by 3 electrometer channels. The evaluation and the fitting of the impedance spectra were carried out with the software ZView (Scribner Inc., USA). At the 280 cm^2 cell the discharges were performed with an electrolyte volume of 2 L at a current density of 40 mA cm^2 (11.5 A) down to a discharge voltage of 0 V, or with 1 L and 40 mA cm^{-2} (2 A) in the 50 cm^2 cell respectively. The linear sweep voltammetry was performed with a potentiostat and an amplifier (Modulab + Booster 12 V, 20 A, Solartron Analytical, USA) with a voltage velocity of 5 mV s^{-1} between open circuit voltage and 0.33 or 0.22 V. All measurements were performed at room temperature.

3. Results and discussion

Fig. 3 shows linear sweep voltammograms and power densities of a 280 cm^2 VOFC at different air flow rates between 1.30 V and 0.33 V. Except at flow rates of 50 mL min^{-1} and 100 mL min^{-1}, the current density increased with decreasing voltage. At flow rates of 50 and 100 mL min^{-1} appeared a current peak at 0.82 V or 0.70 V at −18 mA cm^{-2} and −26 mA cm^{-2} respectively, which could be attributed to a significant limitation of the oxygen reduction reaction (ORR) due to oxygen depletion.

In both curves, the current density decreased after reaching the maximum current density again, then slightly increased, which suggested a different reaction mechanism at low voltages, probably due to hydrogen evolution at low cathode potentials. Beside oxygen depletion limitations, the two curves show even less pronounced differences in the ohmic losses. The maximum power densities at the two flow rates were 14 mW cm^{-2} and 18 mW cm^{-2}. At flow rates of 200 mL min^{-1}–600 mL min^{-1} diminishing limitations were observed, but no peaks in the voltammograms. From 600 mL min^{-1} nearly no differences were visible in the voltammograms with higher flow rates. The voltammograms showed mainly activation and ohmic losses. The maximum power density was at 23 mW cm^{-1}

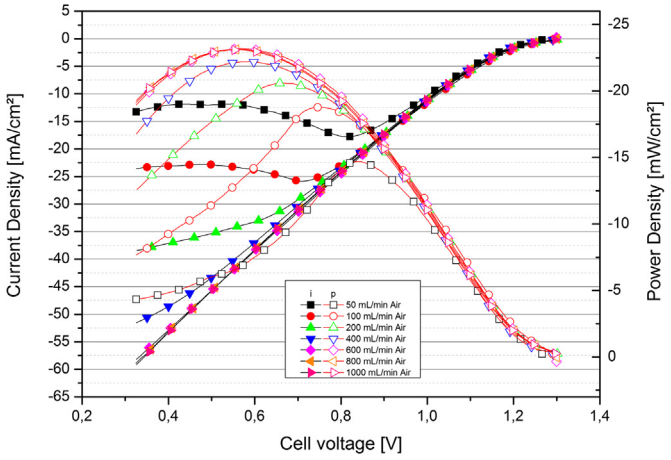

Fig. 3. Linear sweep voltammetry and power density curves at different air volume flows (280 cm^2, 73 mL min^{-1}, 1.6 M V^{2+}).

with 42 mA cm^{-2} and 0.56 V (theoretical faradaic air flow rate at 40 mA cm^{-2} 196 mL min^{-1}). The resistance in the area of the ohmic losses at maximum air flow was calculated to be 14 Ω cm^2, the intersection of the tangent with the *x*-axis was 1.14 V.

Fig. 4 shows the polarization curves and the power density of a VOFC at different flow rates of V^{2+}. The open circuit voltage was 1.28 V and thus with 30 mV, the polarization losses were slightly higher than in the previous study as shown in Fig. 3. The voltammetry curves show at all flow rates primarily activation and ohmic losses, but almost no limitations by mass transport and therefore no limiting current density. The shapes of the curves of the three highest flow rates were nearly parallel, which suggested a polarization difference by charge transfer. The curves of the lower flow rates had different slopes and thus increasing ohmic losses. At a V^{2+} flow rate of 67 mL min^{-1}, the cell achieved a maximum current density of 38 mA cm^{-2} at 0.22 V, while at 180 mL min^{-1}, 59 mA cm^{-2} were obtained. The maximum power densities were 18 mW cm^{-2} at the lowest flow rate and 22 mW cm^{-2} at 0.55 V at the highest flow rate. The resistance in the area of the ohmic losses at maximum flow was calculated to be 15.6 Ω cm^2, the intersection of the tangent with the *x*-axis was calculated to be 1.15 V. Compared with values of Menictas et al. [11], here there were about 33% higher resistance values of ohmic losses, but with 350 mV approximately 43% lower polarization losses for the activation energy.

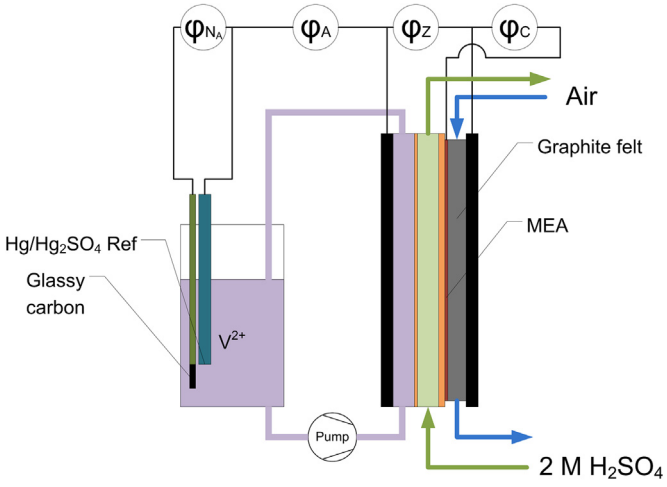

Fig. 2. Schematics of a test setup for the measurement of a 50 cm^2 VOFC.

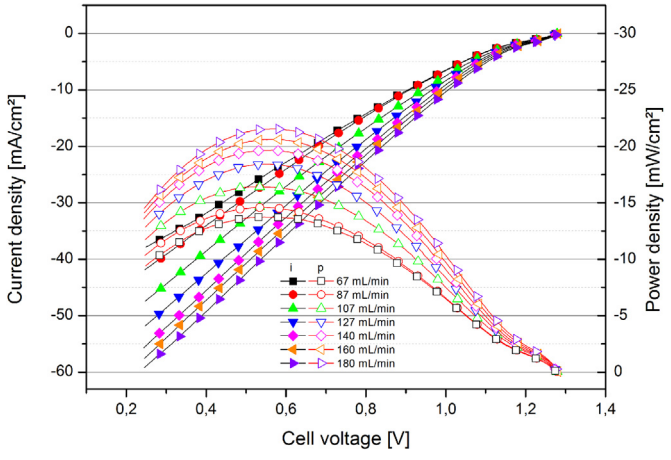

Fig. 4. Linear sweep voltammetry and power density curves at different V^{2+} flows (280 cm^2, 1.6 M V^{2+}, 500 mL min^{-1} air).

Fig. 5 shows the voltages and potentials of a 280 cm^2 and a 50 cm^2 VOFC at a constant discharge current density of 40 mA cm^{-2}. The value of the current density was chosen from the previous measurements, to operate the cell as possible at maximum power. The mass flow ratios λ_V and λ_{Air} of the 280 cm^2 were 30.2 and 5.4 respectively. The 280 cm^2 cell strongly depolarized at the beginning of the discharge from 1.36 V to 0.55 V. Subsequently, the voltage dropped almost linearly down during the discharge time of 4 h, then quickly dropped to the discharge end voltage of 0 V due to V^{2+} concentration depletion. The average cell voltage $\overline{U}$ (Formula (1)) was 0.49 V, the average power density was 19.6 mW cm^{-2}.

$$\overline{U} = \frac{\int_{t_0}^{t_1} U dt}{\Delta t} \tag{7}$$

The converted energy W (Formula (2)) was 18.2% and 23.6 Wh of the theoretical value of 128.8 Wh, corresponding to an energy density of 11.8 Wh L^{-1}.

$$W = I \int_{t_0}^{t_1} U dt \tag{8}$$

The discharge capacity was 49.5 Ah, representing 57.7% (current efficiency) of the theoretical value. The 81.8% loss of energy was caused by capacitive losses on the one hand, as well as by ohmic and activation losses. The proportion of capacity losses was calculated to 36.3 Ah, corresponding to 17.7 Wh (at 0.49 V) and 14% energy loss. The voltage efficiency was 37.8% (Formula (3)) with $\overline{U} = 0.49$ V.

$$\eta_L = \frac{E_{(I)}}{E_0} \tag{9}$$

Without any capacitive loss the converted energy would be 32.1% of the theoretical value 41.3 Wh. The rest of the 67.9% energy loss was due to activation and ohmic losses. The portion of the activation losses could be calculated from the voltage value (1.15 V) of the intersection of the tangent with the *x*-axis as 22.8%. Thus 45.1% ohmic losses made up the main part of the energy loss.

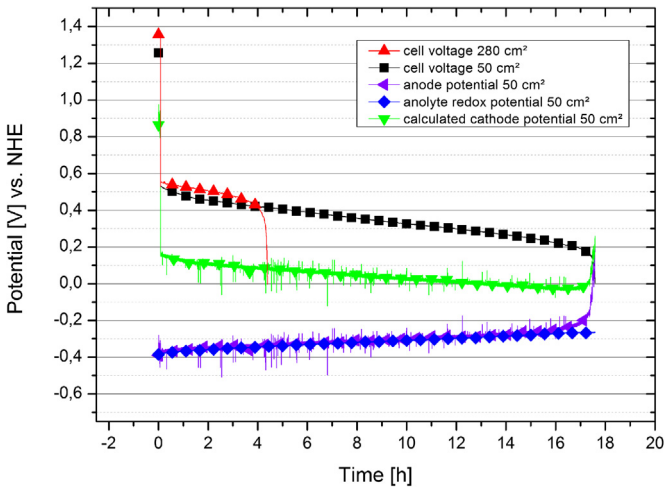

Fig. 5. Voltages and potentials of a 280 cm^2 VOFC (40 mA cm^{-2}, 133 mL min^{-1} 1.6 M V^{2+}, 1000 mL min^{-1} air, 2 L 1.6 M V^{2+}) and a 50 cm^2 VOFC (40 mA cm^{-2}, 43 mL min^{-1} 1.6 M V^{2+}, 100 mL min^{-1} air, 1 L 1.6 M V^{2+}).

The cause of the low discharge capacity may be caused by side reactions, crossover into the intermediate space, handling of the electrolyte, and oxygen diffusion into the plastic based storage container. The high ohmic resistance could be due to the relatively more complex cell setup, especially the contact resistance between the components and the resistance of the second membrane. The high activation loss could be mainly due to water transport problems and a badly formed three phase boundary of the cathode at room temperature. As there is a liquid electrolyte on the other side of the cathode half cell, one may expect diffusion of liquid to the cathode side and thus a negative influence on the three phase boundary in addition to the uptake of product water to the gas stream.

The 50 cm^2 VOFC depolarized quickly during the beginning of the discharge from 1.25 V at OCV to 0.52 V. Compared to the 280 cm^2 VOFC, the average discharge voltage of 0.45 V was 40 mW lower and the OCV was 100 mV lower. The mass flow ratio λ_V and λ_{Air} were 53.8 and 3.0, respectively. The discharge time was 17.5 h, the average power density was 18 mW cm^{-2}, the discharge capacity 35.0 Ah (81.0% of $C_{theor.}$) and the converted energy density 12.0 Wh L^{-1} (18.6% of $W_{theor.}$). Besides the discharge capacity these values were not significantly different from those of the 280 cm^2 VOFC. The higher average discharge voltage of the 280 cm^2 cell compensated the capacitive loss, so that nearly the same values for the energy density were obtained. The respective values of the 50 cm^2 VOFC for the mass flow ratio λ_V was higher and λ_{Air} was lower compared to the 280 cm^2 cell. From the polarization curves in Fig. 4 can be assumed, that the performance of the 280 cm^2 VOFC could be higher at higher λ_V. Should both cell construction have similar behavior, the differences of λ_{Air} should have only caused slight performance changes, since the polarization curves of the 280 cm^2 VOFC in Fig. 3 at air flow rates between 600 mL min^{-1} and 1000 mL min^{-1} had almost identical values.

The shape of the vanadium redox potential of the vanadium solution shown in Fig. 5 showed little difference between the shape of the anode potential. The value of the redox potential was at the beginning of the discharge −0.39 V and −0.28 V at the end. The anode potential differed significantly only at the end of the discharge from the redox potential of the vanadium solution. The value increased to 0.1 V and thus had a difference of 0.38 V to the redox potential. The reaction kinetics of the oxidation of divalent to trivalent vanadium was high during discharge, because only a very low overpotential compared to the redox potential was measured. The observed strong increase of the anode over-potential at the end of the discharge process can be attributed to the depletion of V^{2+} in the anode cycle. The calculated value of the cathode potential decreased sharply by 0.81 V at the beginning of the discharge from 0.98 V to a value of 0.17 V, and decreased further to −0.25 V during the discharge. It only rose back to 0.25 V at the end of the discharge process, following the increase of the anode potential. The cathode potential strongly depolarized from its thermodynamically value of 1.23 V−0.17 V. By contrast the depolarization of the anode potential remained very low throughout the discharging process. The low rate of oxygen reduction at room temperature therefore made the largest contribution to the voltage losses and thus to the performance losses of the two cells.

For a further understanding of the behavior and description of the individual reactions, a simple model with two time constants has been developed (Fig. 6). *R*1 is the ohmic resistance of the cell, and the two time constants represent anode and cathode reactions. By using a constant phase element (CPE) non-ideal capacitive behavior by distribution of relaxation times, due to for example electrode surface effects, were considered. Inductive effects were not considered in the model and accordingly the data was fitted up to a maximum frequency of 3 kHz.

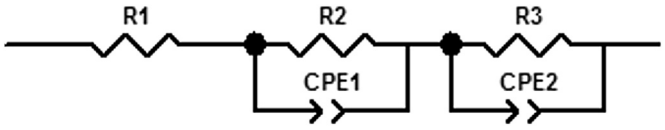

Fig. 6. Applied equivalent circuit to model the impedance spectra.

The impedances were calculated by the following equation:

$$Z(f) = R1 + \frac{R2}{1 + (j2\pi f)^{\alpha 1} Qdl1R2} + \frac{R3}{1 + (j2\pi f)^{\alpha 2} Qdl2R3} \quad (10)$$

Fig. 7 shows the impedance spectra of a charged (OCV = 1.252 V) and an almost fully discharged (OCV = 1.032 V) 280 cm^2 VOFC. Table 1 shows the corresponding fitting values.

With resonant frequencies of approximately 16 or 25 mHz a dominant time constant could be recognized, which was assigned to *R*3/CPE2 in the model. Another time constant occurs at resonance frequencies of 129 or 20 Hz and was assigned to *R*2/CPE1. At frequencies in the range of 2 kHz, a further parameter can be seen that in the discharged state significantly differed from the time constant lying next, which was probably caused by the porous surface, but not taken into account in the model.

In the charged as in the discharged state, the values for the resistor *R*1 changed from 10.4 Ω cm^2 to 9.8 Ω cm^2 only insignificantly. A decrease of *R*1 may be caused by a passage of acid through the membrane and a variation of the three-phase boundary layer. Likewise, changes in contact resistance between GDL and CCM could have led to a decrease of *R*1. The values of the dominant time constant *R*3/CPE2 changed only slightly, but the double layer capacitance Qdl2 decreased significantly by −32%. In the higher-frequency time constant *R*2/CPE1 major changes were observed. The charge transfer resistance *R*2 increased +173% from 3.1 Ω cm^2 to 8.4 Ω cm^2, Qdl1 increased by +131%. Furthermore, the ratio of Qdl1 and Qdl2 in the different charge states differed significantly.

The ratio in the charged state was 1:18.4 and in the discharged state 1:5.6 which suggested a change of the anode and cathode double layer during discharge, probably due to changes of the anode electrode surface, three phase boundary or other ionic species in the double layer. Changing the concentration of divalent vanadium in the anolyte during the discharge should effect a change in a time constant as the time constant, even though the time constant of the oxygen reduction reaction should not affected.

Table 1
Normalized fitting values for a 280 cm^2 VOFC at charged (1.252 V) and discharged state (1.032 V).

Model parameter	Value charged	Error [%]	Value discharged	Error [%]	Change [%]
*R*1 [Ω cm^2]	10.4	0.9	9.8	0.6	−5
*R*2 [Ω cm^2]	3.1	4.4	8.4	2.4	+173
Qdl1 [mF cm^{-2}]	1.9	24.2	4.3	8.4	+131
α1	0.76	4.4	0.67	2.4	−12
*R*3 [Ω cm^2]	246.4	1.4	229.6	1.0	−7
Qdl2 [mF cm^{-2}]	35,0	0.5	24,0	0.6	−32
α2	0.87	0.39	0.95	0.4	+9

If the resonant frequencies are sufficiently apart they can be clearly distinguished in the Bode and Nyquist plots. As previously indicated by reference electrode measurements at VOFCs [15], the dominant high-frequency time constant can be mainly associated with the anode reaction of V^{2+}/V^{3+}, which has been represented herein by *R*2/CPE1 and the ORR at the low-frequency time constant by *R*3/CPE2. The calculated ratios of charge transfer resistance of anode and cathode were 1:79 in the charged state and 1:27 in the discharged state.

Fig. 8 shows the Nyquist and Bode plots of a 280 cm^2 VOFC at different load current densities, in Table 2, the calculated model fitting values are listed. Two time constants are clearly visible in the spectra. The time constant in the frequency range of 1000 Hz–10 Hz was assigned to *R*2/CPE1 and in the range of 10 Hz–0.1 Hz to *R*3/CPE2. As can be seen in Fig. 8b, the values for the resonance frequencies of *R*2/CPE1 were nearly the same at approx. 120 Hz, the *R*2 fitting values were between 3.92 and 4.76 Ω cm^2 and no pattern could be detected. Qdl1 tended to be smaller from 2.9 to 1.4 mF cm^{-2}, but had double-digit fitting errors and α1 had values between 0.57 and 0.71 with no clear trend. The time constant *R*2/CPE1 was almost unchanged. Significant changes in the low-frequency time constant *R*3/CPE2 were observed. Under load, the peaks of the phase shift increased from 0.25 Hz to higher frequencies up to values of about 1 Hz, while the values decreased at the same time. The values of *R*3 decreased significantly from 24.9 Ω cm^2 at −1.8 mA cm^{-2} to about 7 Ω cm^2 at a current density of −10.8 mA cm^{-2}. Qdl2 with values between 34 and 30 mF cm^{-2}, and α2 with values at 0.9, showed no clear changes, which suggested that under these conditions no discernible changes in the cathodic catalyst layer occurred. Like in other PEMFC [17–19], *R*3/CPE2 can be regarded as the double layer capacity (CPE2) and the

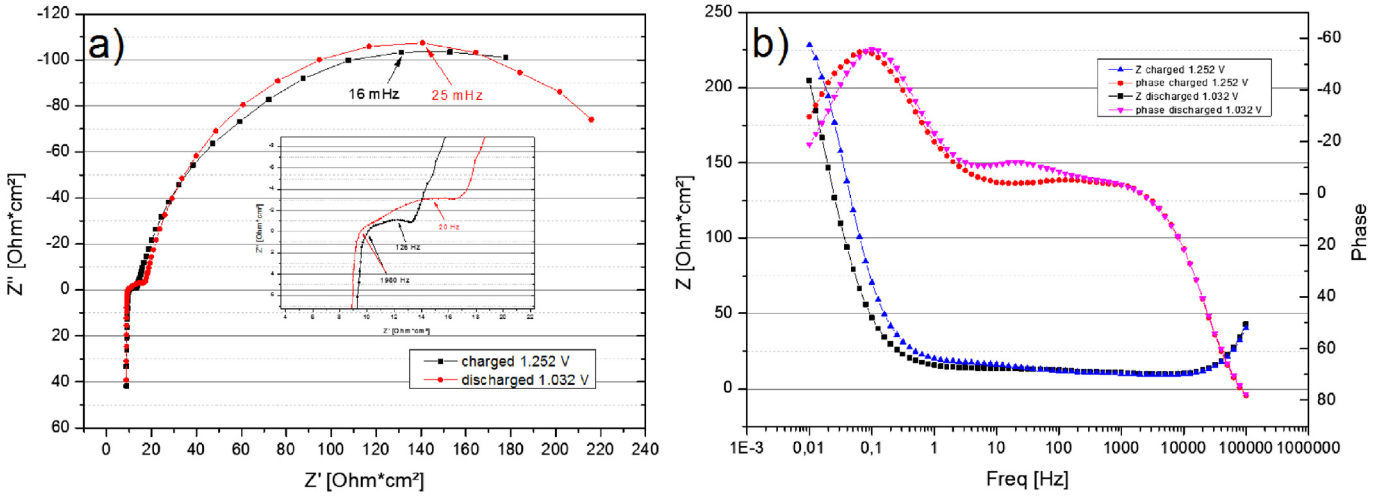

Fig. 7. Nyquist and Bode plots of a 280 cm^2 VOFC at charged (1.252 V) and discharged state (1.032 V).

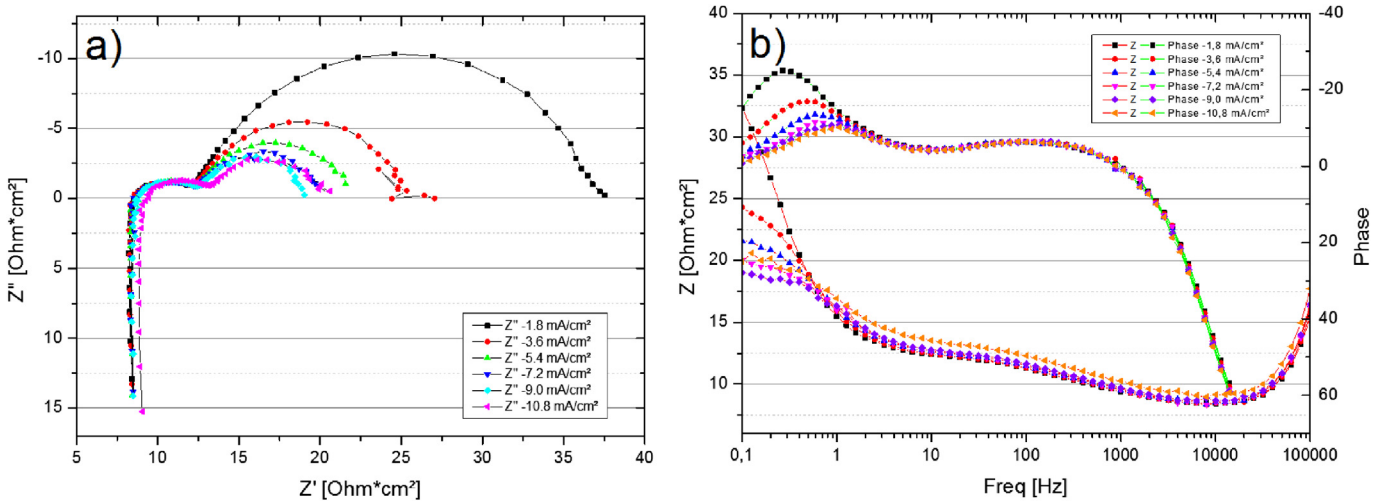

Fig. 8. Nyquist plots (a) und Bode plots (b) of a 280 cm^2 VOFC at different current loads.

charge transfer resistance of the ORR, thereby decreasing values for *R*3 also should have a dependency of the potential at low overvoltages according to the Tafel equation. The ohmic resistance *R*1, with values between 5.3 and 9 Ω cm^2, had more than a decade higher values than in other fuel cells which was caused primarily by a non-optimal configuration of the cell with presumably high contact resistance between the components. Other than the measurements of the charged and discharged VOFC, *R*1 increased from 7.8 Ω cm^2 at −1.8 mA cm^{-2} to 9 Ω cm^2 at −10.8 mA cm^{-2}. We suspect particularly high contact resistance between GDL and CCM, since the two were not hot-pressed and the back pressure from the cavity through the felts used was too low.

The Nyquist plot of a 50 cm^2 VOFC at a load current density of −1.8 mA cm^{-2} shown in Fig. 9, had a similar shape as that of a 280 cm^2 cell. The most significant difference is that the phase angle shift, which decreased continuously, was not observed at the 280 cm^2 cell. The spectra of the anode and cathode impedance also did not show this profile, and the measured impedance and phase angle showed a significant degree of scatter range. However, the phase angle shift was not present in the measurement results of the half-cell impedances, possibly because the two membranes were not measured. The latter was also true for the time constant in the range of 6 Hz–100 Hz, which did not occur in the direct measurement of the half-cell impedances. The fitting values listed in Table 2 were compared to the measured values of the 280 cm^2 cell nearly similar.

The course of the anode impedance predominantly showed ohmic behavior, while the shape of the cathode impedances predominantly showed charge transfer resistance. The value of the measured charge transfer resistance of the cathode was 12.9 Ω cm^2, and therefore under consideration of the fitting error, similar to the value of the whole cell (15.8 Ω cm^2), but 32% lower than the value of the 280 cm^2 cell. The ohmic resistance of the 50 cm^2 cell with a value of 5.3 Ω cm^2, was also 32% lower than the value of the 280 cm^2 cell (7.8 Ω cm^2), which explains the slightly better performance of the 280 cm^2.

4. Conclusions

A VOFC with an active area of 280 cm^2 and two membranes was constructed and compared with a 50 cm^2 cell. In addition to the cell voltage, anode and cathode potentials could be recorded in the 50 cm^2 VOFC to obtain a deeper understanding of the influences on the half-cell reaction rates. The maximum power density of the 280 cm^2 cell was 23 mW cm^{-2}. During a discharge of 2 L 1.6 M V^{2+} solution with a current density of 40 mA cm^{-2}, the 280 cm^2 cell achieved an average power density of 19.6 mW cm^{-2}, while the 50 cm^2 cell achieved an average power density of 18 mW cm^{-2}. Both cells had similar values of voltage efficiencies and impedances, suggesting a nearly equivalent upscaling of the 280 cm^2 relative to the half-cell reactions. However, the current efficiencies of the 280 cm^2 cell were significantly lower than those of the 50 cm^2 cell,

Table 2
Normalized impedance model fitting values for a 280 cm^2 and a 50 cm^2 VOFC at different current densities.

Model parameter	−1.8 mA cm^2	−1.8 mA cm^{-2} 50 cm^2 cell	−1.8 mA cm^{-2} 50 cm^2 cathode	−3.6 mA cm^{-2}	−5.4 mA cm^{-2}	−7.2 mA cm^{-2}	−9.0 mA cm^{-2}	−10.8 mA cm^{-2}
*R*1 [Ω cm^2]	7.84	5.3	–	8.68	8.12	8.4	8.4	8.96
Error [%]	1.2	–	–	1.1	0.9	0.9	0.9	0.9
*R*2 [Ω cm^2]	4.76	7.2	–	3.92	4.76	3.92	4.48	4.48
Error [%]	3.7	4.3	–	4.5	3.2	3.9	3.4	3.8
*Q*dl1 [mF cm^{-2}]	2.9	5.4	–	1.6	2.2	1.2	1.7	1.4
Error [%]	15.9	8.9	–	22.7	11.8	18.9	13.0	15.5
α1	0.57	0.72	–	0.7	0.61	0.71	0.64	0.67
Error [%]	5.4	2.3	–	4.8	4.7	4.2	4.6	4.7
*R*3 [Ω cm^2]	24.9	15.8	16.9	12.9	9.5	7.6	6.4	7
Error [%]	1.0	2.6	10.5	1.5	2.3	2.8	3.0	3.0
*Q*dl2 [mF cm^{-2}]	34.0	49.5	22.3	31.4	31.8	29.3	30.0	30.4
Error [%]	1.4	2.3	13.4	2.3	2.7	3.7	3.9	4.0
α2	0.9	1.0	0.96	0.9	0.9	0.9	0.91	0.88
Error [%]	1.0	1.5	5.3	1.5	2.0	2.4	2.5	2.8

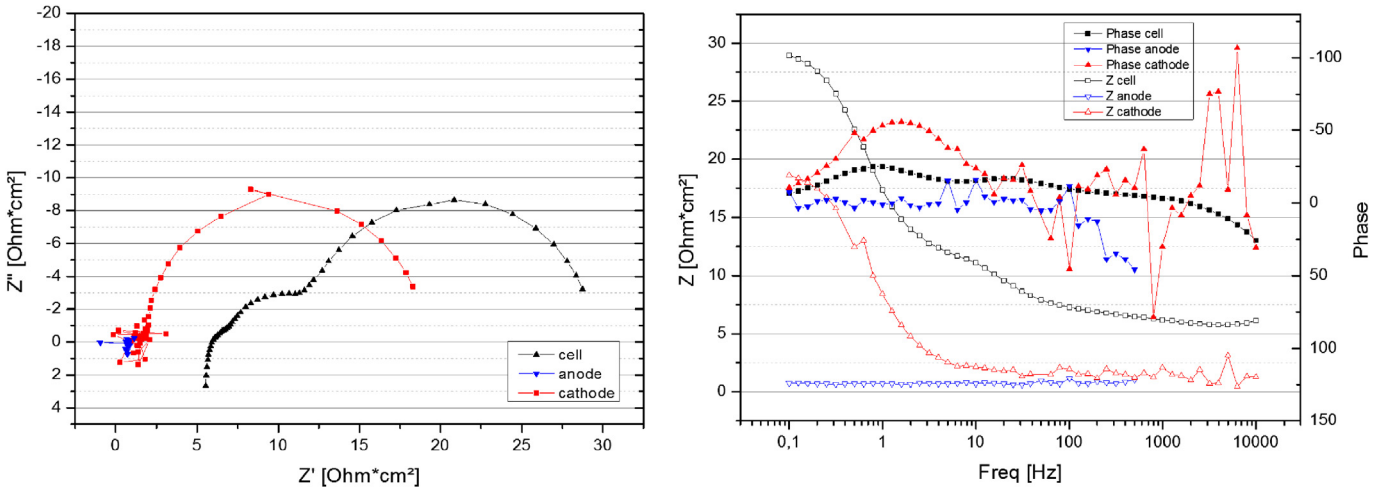

Fig. 9. Nyquist and Bode plots of a 50 cm^2 VOFC at a load current density of −1.8 mA cm^{-2} (black – cell, red – cathode, blue – anode). (For interpretation of the references to color in this figure legend, the reader is referred to the web version of this article.)

which has been attributed to side reactions. In both cells, the oxygen reduction reaction was considerably slower than V^{2+} oxidation, which was caused mainly by the low reaction rate at room temperature and also by non-optimized cathode half-cells. Due to high contact resistance, probably in particular those between CCM and GDL, the ohmic resistances of the two cells were more than a decade larger than in other PEMFCs. Due to the low kinetics of ORR at room temperature, the large proportion of side reactions and the high cell resistance, with 11.8 Wh L^{-1} an energy density of only 18.2% of the theoretical value of 64.4 Wh L^{-1} was achieved.

Acknowledgments

The authors gratefully acknowledge the Ministry of Finance and Economics of the Federal State of Baden-Württemberg for financing this project.

References

[1] T. Rehrl, R. Friedrich, Energy Policy 34 (2006) 2413–2428.
[2] Encyclopedia of Electrochemical Power Sources, Elsevier B.V., The Netherlands, 2009.
[3] T. Ohzuku, A. Ueda, N. Yamamoto, J. Electrochem. Soc. 142 (1995) 1431–1435.
[4] Y.-S. Lin, J.-G. Duh, J. Power Sources 196 (2011) 10698–10703.
[5] K. Amine, I. Belharouak, Z. Chen, T. Tran, H. Yumoto, N. Ota, S.-T. Myung, Y.-K. Sun, Adv. Mater. 22 (2010) 3052–3057.
[6] W. Qian, D.P. Wilkinson, J. Shen, H. Wang, J. Zhang, J. Power Sources 154 (2006) 202–213.
[7] A. Ryu, J. Photochem. Photobiol. C Photochem. Rev. 11 (2010) 179–209.
[8] M. Skyllas-Kazacos, M.H. Chakrabarti, S.A. Hajimolana, F.S. Mjalli, M. Saleem, J. Electrochem. Soc. 158 (2011) R55–R79.
[9] W. Wang, Q. Luo, B. Li, X. Wei, L. Li, Z. Yang, Adv. Funct. Mater. 23 (2012) 970–986.
[10] H. Kaneko, A. Negishi, K. Nozaki, K. Sato, M. Nakajima, US Patent 5318865, 1992.
[11] C. Menictas, M. Skyllas-Kazacos, J. Appl. Electrochem. 41 (2011) 1223–1232.
[12] S.S. Hosseiny, M. Saakes, M. Wessling, Electrochem. Commun. 13 (2011) 751–754.
[13] J. Noack, C. Cremers, K. Pinkwart, J. Tuebke, in: 218th ECS Meeting, 10–15 October 2010. Las Vegas, NV.
[14] J. Noack, T. Berger, K. Pinkwart, J. Tübke, German Patent DE 102011107185, 2011.
[15] J. Noack, J. Tuebke, in: 3rd International Flow Battery Forum, 2012. Munich, Germany.
[16] G. Li, P.G. Pickup, Electrochim. Acta 49 (2004) 4119–4126.
[17] S. Asghari, A. Mokmeli, M. Samavati, in: The 1st Iranian Conference On Hydrogen & Fuel Cell, vol. 35, 2010, pp. 9283–9290.
[18] C.-M. Lai, J.-C. Lin, K.-L. Hsueh, C.-P. Hwang, K.-C. Tsay, L.-D. Tsai, Y.-M. Peng, Int. J. Hydrogen Energy 32 (2007) 4381–4388.
[19] X. Yan, M. Hou, L. Sun, D. Liang, Q. Shen, H. Xu, P. Ming, B. Yi, Fuel Cells 32 (2007) 4358–4364.